Nonstandard relaxation behavior in ionically conducting materials

Philipp Maass*
Institut für Physikalische Chemie und Elektrochemie, Universität Hannover, Callinstrasse 3-3a, 30167 Hannover, Germany

Martin Meyer and Armin Bunde
Institut für Theoretische Physik, Justus-Liebig Universität Giessen, Heinrich-Buff-Ring 16, 35392 Giessen, Germany
(Received 1 August 1994)

We investigate by Monte Carlo simulations the diffusion of ions in ordered and structurally disordered lattices, where the Coulomb interaction between the mobile ions is explicitly taken into account. Results for tracer diffusion, conductivity, the diffusion-induced spin-lattice relaxation rate, and the incoherent intermediate scattering function are discussed in detail. It is shown that the presence of both disorder and Coulomb interactions leads to the typical deviations from the standard behavior of the relevant transport quantities (non-BPP, where BPP indicates Bloembergen, Purcell, and Pound behavior of the spin-lattice relaxation rate, strong dispersion of the conductivity, nonexponential decay of relaxation functions, etc.) that are experimentally observed in a wide class of ion-conducting materials.

I. INTRODUCTION

The low-frequency dynamic response of many nonmetallic materials is governed by the transport of mobile ions or other charged mobile defects. The classes of such materials include traditional ionic glasses, polymeric and glassy superionic conductors, highly defected crystals, or even highly viscous liquids such as glass-forming melts. To get an understanding of the microscopic transport mechanism in these materials, a large number of experimental techniques has been applied; among them are tracer experiments,[1] conductivity measurements (modulus spectroscopy),[2–4] nuclear spin-lattice relaxation,[5–7] quasielastic neutron scattering,[8,9] internal friction, and ultrasonic absorption measurements (Brillouin scattering).[10,11] In all these experiments the measured quantities show characteristic deviations from the standard behavior that one would expect for a purely random motion of the mobile ions.

For example, the dynamic conductivity $\hat{\sigma}(\omega)$ in ionically conducting solids exhibits, for fixed temperature T, a dc plateau at low frequencies (below some crossover frequency $1/\tau_\sigma$), and follows an approximate power-law behavior at larger frequencies,[12]

$$\hat{\sigma}(\omega)\sim\begin{cases}\sigma_{\rm dc}, & \omega\tau_\sigma\ll 1,\\ (i\omega)^{n_\sigma}, & \omega\tau_\sigma\gg 1.\end{cases}\tag{1}$$

The dispersive regime ($\omega\tau_\sigma\gg 1$) usually continues up to phonon frequencies and the exponent $n_\sigma>0$ tends to increase on lowering the temperature. From standard random-walk theory, one would expect no dispersion to occur, i.e., $n_\sigma=0$ (see Sec. II B). In both the dc and the dispersive regimes, $\hat{\sigma}(\omega)$ is thermally activated, where the activation energy E_1^σ for the dc conductivity is always larger than the apparent activation energy E_2^σ in the dispersive regime, $E_1^\sigma>E_2^\sigma$. The crossover frequency τ_σ^{-1}, which separates the two regimes, is also thermally activated with an activation energy E_σ approximately equal to E_1^σ. This overall behavior is not restricted to ionically conducting solids but occurs also in disordered electronic conductors such as amorphous semiconductors, electronic conducting polymers, and disordered polaronic conductors. The widespread occurrence of such similar low-frequency dielectric behavior in all disordered solids was pointed out by Jonscher[13] and is known as the "universal dielectric response."

Apart from dielectric measurements, perhaps the most common experimental technique to probe ionic motion in disordered media is nuclear magnetic resonance (NMR). The behavior of the diffusion-induced spin-lattice relaxation rate $1/T_1(\omega,T)$, as a function of temperature T and Larmor frequency ω, can be summarized as follows:

$$\frac{1}{T_1}(\omega,T)\sim\begin{cases}\exp(E_1^{\rm NMR}/k_BT), & T\gg T_{\max}(\omega),\\ \omega^{n_{\rm NMR}-2}\exp(-E_2^{\rm NMR}/k_BT), & T\ll T_{\max}(\omega),\end{cases}\tag{2}$$

with an exponent $n_{\rm NMR}\geq 0$. In an Arrhenius plot, $1/T_1$ shows a maximum at $1/T_{\max}(\omega)$, where the temperature $T_{\max}(\omega)$ decreases with decreasing frequency. Since generally $E_1^{\rm NMR}>E_2^{\rm NMR}$, the curve is asymmetric in shape. For fixed temperature T, $1/T_1(\omega,T)$ is constant at low frequencies $\omega\ll 1/\tau_{\rm NMR}$ and decreases as $\omega^{n_{\rm NMR}-2}$ for $\omega\gg 1/\tau_{\rm NMR}$. The NMR correlation time $\tau_{\rm NMR}$ is considerably larger than the inverse hopping rate of the mobile ions.[14] In contrast to this overall behavior, the standard Bloembergen-Purcell-Pound (BPP) theory[15] predicts a symmetric maximum of $1/T_1$ in the Arrhenius plot with $n_{\rm NMR}=0$ and a NMR crossover time $\tau_{\rm NMR}$ of the order of the inverse hopping rate (see Sec. II D).

Dynamic scattering of neutrons is a much more extensive technique to investigate the ionic transport. In many

structurally disordered ionic conductors broad quasielastic components in the scattering spectra are observed. The line shapes of these components often deviate from simple Lorentzians, which are expected in the simple random-walk case (see Sec. II C). A similar behavior has been found in mechanical loss spectroscopy.[10,11] The spectra are usually much broader than simple Debye spectra, reflecting an inherent nonexponential nature of the ionic relaxation processes.

From a theoretical point of view, the ionic transport in solids is a very complex phenomenon and rigorous solutions are not available. For an ordered host lattice a mode-coupling theory has been developed to study the effect of long-range Coulomb interactions between the mobile ions,[16] but is has turned out recently that the disorder also plays an essential role in describing the experimental situation properly.[17,18] A rigorous solution of this complex problem is impossible to obtain, and various phenomenological and semimicroscopic approaches have been successfully applied. Prominent examples are the coupling scheme proposed by Ngai,[19] the jump relaxation model pioneered by Funke,[8] and the diffusion-controlled relaxation model elaborated by Elliott and Owens.[20] Attempts have been made to map the dynamics of the many-body problem onto the dynamics of a single particle moving in a complex energy landscape.[21–23]

For a more microscopic description of the ionic transport one is dependent upon numerical investigations. In this paper we summarize the results of a detailed Monte Carlo study of a simple lattice-gas model by which the effect of both long-range Coulomb interactions between the mobile ions and structural disorder in the host lattice is investigated in a systematic way. In contrast to other methods (e.g., molecular-dynamic simulation), the Monte Carlo method is not restricted to the short-time regime of the ion dynamics and can explore the behavior of the basic quantities for the relevant time and frequency scales.

The paper extends earlier work[17,18] and is organized as follows. In Sec. II we define the basic quantities that we will investigate and discuss their standard behavior, assuming that each mobile particle performs a simple random walk and does not interact with the other mobile particles. In Sec. III we present the Coulomb lattice-gas model and explain the simulation technique. In Sec. IV we discuss the numerical results. Section V finally concludes the paper with a brief summary and discussion.

II. BASIC QUANTITIES

In this section we discuss the standard behavior of the basic quantities of interest. We assume that the mobile particles do not interfere with each other and perform simple random walks on a d-dimensional (cubic) lattice with lattice constant a. The lattice has length L and the particle density is $\rho=N/L^d$, where N is the number of particles. We assume that the particles perform thermally activated hops among nearest-neighbor sites of the lattice. The mean residence time τ_0 between two jumps of a particle is $\tau_0=\tau_\infty \exp(V_0/k_BT)$, where τ_∞ is a rattling time and V_0 is the structural energy barrier between two nearest-neighboring lattice sites.

A. Tracer diffusion

The tracer diffusion coefficient D is related to the long-time limit of the mean square displacement $\langle r^2(t)\rangle$ of a tracer particle, $D=\lim_{t\to\infty}\langle r^2(t)\rangle/2dt$. Experimentally, D can be obtained from the concentration profile of radioactive tracers introduced into the material under investigation.

It is convenient to define a generalized frequency-dependent tracer diffusion coefficient $\hat{D}(\omega)$ by

$$\hat{D}(\omega)=-\frac{\omega^2}{2d}\lim_{\epsilon\to+0}\int_0^\infty \langle r^2(t)\rangle e^{i\omega t-\epsilon t}dt\ , \tag{3}$$

which for $\omega\to 0$ approaches D.

If the particles perform simple random walks, subsequent jumps of a tracer particle are uncorrelated and the mean square displacement increases linearly with time according to Ficks law, $\langle r^2(t)\rangle=a^2t/\tau_0$, yielding $\hat{D}(\omega)=D=a^2/2d\tau_0$, independent of frequency. If the particle hops are correlated, $\langle r^2(t)\rangle$ only increases linearly for very small and very large times, and one can define a tracer correlation factor $f_{\rm tr}$ as the ratio of the long-time diffusion coefficient D and the short-time diffusion coefficient $D_{\rm ST}$ by $f_{\rm tr}\equiv D/D_{\rm ST}$. The deviation of $f_{\rm tr}$ from unity can be regarded as a measure of the strength of the correlations. If a particle prefers to jump back to the site where it came from (backward correlations) $f_{\rm tr}<1$; if it prefers to jump forward (forward correlations), we have $f_{\rm tr}>1$.

B. Dynamic conductivity

The dynamic conductivity $\hat{\sigma}(\omega)$ describes the linear response of the current density to an external electric field and it is related to the autocorrelation function $\langle \mathbf{j}(t)\cdot\mathbf{j}(0)\rangle$ of the current density in the absence of the electric field (Kubo formula[24]):

$$\hat{\sigma}(\omega)=\frac{L^d}{dk_BT}\lim_{\epsilon\to+0}\int_0^\infty \langle \mathbf{j}(t)\cdot\mathbf{j}(0)\rangle e^{i\omega t-\epsilon t}dt\ . \tag{4}$$

The brackets $\langle\ \rangle$ denote a thermal average and the current density is given by the sum over the particle velocities, $\mathbf{j}(t)=(e\rho/N)\sum_{i=1}^N \mathbf{v}_i(t)$, where e is the charge of the particles. (For noninteracting particles the charge e means only a formal coupling to the external electric field.) Separating the velocity autocorrelation function

$$\langle \mathbf{v}_i(t)\cdot\mathbf{v}_i(0)\rangle\equiv\langle \mathbf{v}(t)\cdot\mathbf{v}(0)\rangle$$

from the cross-correlation part in the autocorrelation function of the current density, we can write

$$\langle \mathbf{j}(t)\cdot\mathbf{j}(0)\rangle=\frac{\rho e^2}{L^d}\left[\langle \mathbf{v}(t)\cdot\mathbf{v}(0)\rangle+\frac{1}{N}\sum_{i\neq j}^{N}\langle \mathbf{v}_i(t)\cdot\mathbf{v}_j(0)\rangle\right]. \tag{5}$$

In the absence of mutual interactions between the mobile particles, $\langle \mathbf{v}_i(t)\cdot\mathbf{v}_j(0)\rangle=0$ for $i\neq j$ and $\hat{\sigma}(\omega)$ is simply related to $\hat{D}(\omega)$ via the Nernst-Einstein relation

$$\hat{\sigma}(\omega)=\frac{\rho e^2}{k_B T}\hat{D}(\omega) . \tag{6}$$

For the simple random-walk case, this yields $\hat{\sigma}(\omega)=\rho e^2 a^2/2dk_B T\tau_0$ independent of ω.

For interacting particles the cross correlations do not vanish and Eq. (6) is no longer valid. We define a generalized frequency-dependent Haven ratio $\hat{H}_R(\omega)$ by

$$\hat{H}_R(\omega)=\frac{\rho e^2}{k_B T}\frac{\hat{D}(\omega)}{\hat{\sigma}(\omega)} , \tag{7}$$

which is a measure of the strength of the cross correlations at frequency ω. For frequencies ω larger than the hopping rate the cross correlations vanish even if the particles interact and $\hat{H}_R(\omega)$ approaches 1. In the limit $\omega\to 0$, $\hat{H}_R(\omega)$ approaches the ordinary Haven ratio $H_R=\rho e^2 D/k_B T\sigma_{\rm dc}$.

C. Probability distribution and incoherent neutron scattering

For a more detailed description of the diffusion process, one considers the distribution function $P(r,t)$, which denotes the probability for an ion to be on a (lattice) site $\mathbf{r}$ at time t, if it started at $t=0$ from site $\mathbf{0}$. The Fourier transform of $P(\mathbf{r},t)$ is the incoherent structure factor $S_{\rm inc}(\mathbf{k},\omega)$,

$$S_{\rm inc}(\mathbf{k},\omega)=\frac{1}{2\pi}\int d\mathbf{r}\int dt\, P(\mathbf{r},t)e^{-i(\mathbf{k}\cdot\mathbf{r}-\omega t)} \equiv\frac{1}{2\pi}\int dt\, S_{\rm inc}(\mathbf{k},t)e^{i\omega t} , \tag{8}$$

which contributes to the differential cross section obtained in scattering experiments.

For simple random walks on a Bravais lattice, the intermediate scattering function $S_{\rm inc}(\mathbf{k},t)$ decays exponentially,

$$S_{\rm inc}(\mathbf{k},t)=\exp\left[-\Lambda(\mathbf{k})\frac{|t|}{\tau_0}\right] , \tag{9}$$

with $\Lambda(\mathbf{k})=\sum_{\mathbf{d}}[1-\cos(\mathbf{dk})]/\nu$, where the sum runs over all nearest-neighbor vectors $\mathbf{d}$ and ν is the number of nearest neighbors. Accordingly, $S_{\rm inc}(\mathbf{k},\omega)$ is a simple Lorentzian with width $\Lambda(\mathbf{k})/\tau_0$.

For $t/\tau_0\gg r/a$, $P(\mathbf{r},t)$ is a Gaussian with width $R(t)\equiv\langle r^2(t)\rangle^{1/2}$,

$$P(\mathbf{r},t)=\left[\frac{d}{2\pi R^2(t)}\right]^{d/2}\exp\left[-\frac{dr^2}{2R^2(t)}\right] . \tag{10}$$

D. Spin-lattice relaxation

In an external static magnetic field H, the alignment of the nuclear magnetic moments of the mobile ions gives rise to a total magnetization in the direction of the applied field. By a radio-frequency pulse perpendicular to the static field this magnetization can be rotated into the opposite direction. Fluctuating local magnetic and electric fields cause the magnetization to relax into the original direction parallel to the static field H in a characteristic time T_1. The spin-lattice relaxation rate $1/T_1$ depends on both the magnitude of the field H and the temperature T.

In the case of ionic conductors mainly two mechanisms give rise to the fluctuating local fields:

(i) the magnetic dipole-dipole interaction between the mobile particles;

(ii) the interaction of the nuclear quadrupolar moment of one particle with the electric field gradient of another particle (as long as the ions have nuclear spin larger than $\frac{1}{2}$ and the quadrupole moment of the nucleus does not vanish).

According to the standard theory,[25,26] $1/T_1$ is determined by the spectral densities $J^{(1)}(\omega)$ and $J^{(2)}(\omega)$,

$$\frac{1}{T_1}=C[J^{(1)}(\omega)+J^{(2)}(2\omega)] , \tag{11}$$

where $\omega=\gamma H$ is the Larmor frequency. The spectral densities are the Fourier transforms of the NMR correlation functions $G^{(q)}(t)$,

$$J^{(q)}(\omega)=\int_{-\infty}^{\infty}G^{(q)}(t)e^{i\omega t}dt, \quad q=1,2 . \tag{12}$$

In both cases (i) and (ii) the correlation functions $G^{(q)}(t)$ can be written as[26]

$$G^{(q)}(t)=\frac{1}{N}\sum_{i\neq j}^{N}\langle F_{ij}^{(q)*}(t)F_{ij}^{(q)}(0)\rangle , \tag{13}$$

where

$$F_{ij}^{(q)}(t)=q(8\pi/15)^{1/2}Y_2^q[\Omega_{ij}(t)]/r_{ij}^3(t)$$

is the local field between the particles i and j. Y_2^q are the spherical harmonics, and Ω_{ij} and r_{ij} are the spherical coordinates of the vector $\mathbf{r}_{ij}$ pointing from particle i to particle j, with respect to the magnetic field. The constant C in (11) depends on the nuclear properties of the mobile particles, $C=\frac{3}{2}\gamma^4\hbar^2 I(I+1)$ in case (i) and

$$C=\tfrac{3}{2}(e^2Q/\hbar)^2 I(I+1)/[I(2I-1)]^2$$

in case (ii). Here γ is the gyromagnetic ratio, I the spin, and Q the quadrupolar moment of the nucleus.

The ansatz $G^{(q)}(t)=G^{(q)}(0)e^{-t/\tau_0}$, commonly referred to as the BPP ansatz, leads to

$$\frac{1}{T_1}=CG^{(1)}(0)\left[\frac{\tau_0}{1+(\omega\tau_0)^2}+\frac{4\tau_0}{1+(2\omega\tau_0)^2}\right] , \tag{14}$$

where we have used $G^{(2)}(0)=4G^{(1)}(0)$, valid for an isotropic distribution of the ions.[25] In an Arrhenius plot of $\ln 1/T_1$ versus inverse temperature, the curve is symmetric in shape with activation energies equal to V_0 and $-V_0$ on the high- and low-temperature sides of the $1/T_1$ maximum, which occurs at $\omega\tau_0\approx 1$. At the low-temperature side ($\omega\tau_0\gg 1$), $1/T_1$ decreases as $\omega^{-2}=(\gamma H)^{-2}$ with increasing field H.

In the Appendix we show that for simple random walks the *asymptotic* decay of $G^{(q)}(t)$ is algebraic rather than exponential. However, for Eq. (14) to be approximately valid it is sufficient that the correlation functions decay linearly with t for small times and faster than $1/t$

for large times. Since both conditions are satisfied in the simple random-walk case (for $d=3$), the deviations from the exponential decay do not lead to pronounced changes of the standard behavior of $1/T_1$, Eq. (14).

III. MODEL AND NUMERICAL TECHNIQUE

As discussed in the Introduction, in most cases strong deviations from the standard behavior are experimentally observed. We will show below that, for a more realistic description of the ionic transport that goes beyond the simple random-walk case, one has to take into account at least (a) the Coulomb interaction between the mobile charge carriers and (b) the structural disorder of the host system. The influence of the immobile counterions on the ionic transport is not studied explicitly.[27] To ensure the charge neutrality of the whole system we treat the counterions as a smeared, spatially homogeneous charge distribution.

To model the structural disorder in the host lattice in a most simple way we assume that only a fraction p of lattice sites is accessible for the mobile ions; the rest of the sites are blocked. This model is known as the site percolation model.[28] For p well above the percolation threshold p_c ($p_c \cong 0.312$ for the sc lattice), most of the accessible sites belong to the "infinite percolation cluster" (IPC), which connects opposite sides of the lattice. We disregard the small finite clusters of accessible sites in the system and consider as our model for structural disorder only the IPC, where all mobile ions exhibit long-range mobility. This disordered structure of accessible sites is reminiscent of a "connective tissue" or a "crumpled handkerchief," which has been suggested to model diffusion paths in ionic glasses.[29] Figure 1 shows a two-dimensional illustration of the model system.

FIG. 1. Two-dimensional illustration of the disordered substrate with $p=0.65, L=50, \rho=0.05$, and $\Gamma=40$. Blocked sites are black and available sites white. Open circles symbolize the particles.

In the detailed numerical procedure we choose a simple cubic lattice of length L with lattice constant a and use periodic boundary conditions. A fraction $1-p$ ($p>p_c$) of the lattice sites is randomly blocked and the IPC is determined with the help of the Hoshen-Kopelmann algorithm.[30] Then the sites of the IPC are randomly occupied by $N=\rho L^3$ mobile ions with charge e, where ρ is the ion density. Double occupancy of sites is forbidden. The strength of the Coulomb interaction relative to the thermal energy $k_B T$ is conveniently characterized by the plasma parameter $\Gamma \equiv e^2/(r_s k_B T)$, where $\frac{4}{3}\pi r_s^3 = \rho^{-1}$. The strength relative to the structural potential barrier V_0 is $\eta \equiv e^2/(r_s V_0)$.

To model the diffusion process we use a standard Monte Carlo algorithm. In each elementary step of the simulation, an ion is chosen randomly, and a nearest-neighbor site is also chosen, to which the ion attempts to jump. If the neighboring site is blocked or occupied by another ion, the jump is rejected. If the neighboring site is vacant, the ion jumps to it with probability $w=1$, if the change ΔE in energy of the ionic subsystem caused by the jump is negative. If $\Delta E>0$, the ion jumps with probability $w=\exp(-\Delta E/k_B T)$. The transition energy ΔE for a jump trial of particle i at position $\mathbf{r}_i$ to a vacant nearest-neighbor site at position $\mathbf{r}_i+\mathbf{u}$ is given by

$$\Delta E = e^2 \sum_{j\neq i} \sum_{\mathbf{n}} \left[\frac{1}{|\mathbf{r}_i+\mathbf{u}-\mathbf{r}_j+L\mathbf{n}|} - \frac{1}{|\mathbf{r}_i-\mathbf{r}_j+L\mathbf{n}|} \right], \tag{15}$$

where the inner sum runs over all triples $\mathbf{n}=(n_1,n_2,n_3)$ of whole numbers and refers to the image charges caused by the periodic boundary conditions. This inner sum is conditionally convergent and can be calculated by using Ewald's method.[31] To save computing time the sum is evaluated before the simulation and stored for all possible pair vectors $\mathbf{r}_{ij}=\mathbf{r}_i-\mathbf{r}_j$ and jump directions $\mathbf{u}$. After each elementary step, the time t is incremented by τ_0/N, where $\tau_0=\tau_\infty \exp(V_0/k_B T)$ is the mean residence time between two jumps of an ion in the absence of Coulomb interactions and structural disorder (see Sec. II).

The elementary simulation step is repeated again and again, until thermal equilibrium is reached, where the total energy of the ionic subsystem fluctuates around a constant mean value. After thermalization the quantities of interest are determined.

To obtain the mean square displacement $\langle r^2(t)\rangle$, all particle positions $\mathbf{r}_i(0)$ are stored at time $t=0$ after thermalization. At time t, the particles are at positions $\mathbf{r}_i(t)$, and the mean square displacement is calculated from

$$\langle r^2(t)\rangle = (1/N) \sum_{i=1}^{N} [\mathbf{r}_i(t)-\mathbf{r}_i(0)]^2 .$$

To obtain the NMR correlation functions $G^{(q)}(t)$, the magnetic field H is aligned along the z direction and all pair vectors $\mathbf{r}_{ij}(0)$ are stored at time $t=0$ using the minimum image convention.[31] At time t these pair vec-

tors are $\mathbf{r}_{ij}(t)$ and the $G^{(q)}(t)$ are calculated according to Eq. (13).

The frequency-dependent conductivity is determined by the current response to a (small) external sinusoidal electric field $E(t)=E_0\sin(\omega t)$ aligned in the x direction. The effect of the field is taken into account by the way the neighboring site is chosen to which an ion attempts to jump (see above). In the absence of the electric field, the six nearest-neighbor sites are equivalent and are chosen with equal probability $\frac{1}{6}$. In the presence of the field, the sites in the $\pm x$ direction are chosen with probability $[1\pm\epsilon(t)]/6$, where $\epsilon(t)\equiv eE(t)a/2k_BT\ll 1$. The resulting current density $J(t)$ in the x direction is determined by counting the number $N_+(t)$ and $N_-(t)$ of jumps in the $+x$ and $-x$ direction in a small time interval $t-\Delta t/2\le t<t+\Delta t/2$, where $\Delta t\ll 2\pi/\omega$. The mean values of $N_+(t)$ and $N_-(t)$, averaged over several samples, determine the mean current density

$$J(t)=ea[\langle N_+(t)\rangle-\langle N_-(t)\rangle]/L^3$$

and, since $J(t)$ can be written as

$$J(t)=\sigma'(\omega)E_0\sin(\omega t)-\sigma''(\omega)E_0\cos(\omega t)\ ,$$

the real and imaginary parts $\sigma'(\omega)$ and $\sigma''(\omega)$ of the frequency-dependent conductivity.

In order to improve the statistics, the results are finally averaged over typically 100 thermalized configurations.

IV. NUMERICAL RESULTS

Most of our numerical simulations have been performed for a simple cubic lattice of length $L=39a$, fixed ion density $\rho=10^{-2}/a^3$, and fixed $\eta=e^2/(r_sV_0)=5$, which defines our set of standard parameters. To investigate the effect of disorder, we compare results for the ordered lattice ($p=1$) with those for the disordered substrate ($p=0.4$). The strength of the Coulomb interactions, represented by the plasma parameter Γ, is varied by changing the temperature.

Figures 2(a) and 2(b) show the time-dependent diffusion coefficient $D(t)\equiv\langle r^2(t)\rangle/2dt$ in units of $D_0\equiv a^2/2d\tau_0$ as a function of t/τ_0 for $\Gamma=0$, 40, and 80 in (a) the ordered lattice ($p=1$) and (b) the disordered system ($p=0.4$). For $t/\tau_0\ll 1$, $\langle r^2(t)\rangle$ is proportional to the total number of successful hops, which increases linearly with time and therefore $D(t)$ is constant, $D(t)=D_{\rm ST}$. For $t/\tau_0>1$, $D(t)$ decreases with time t and finally approaches $D_{\rm tr}$. In the ordered system, the decrease of $D(t)$ is comparatively weak, even at large plasma parameters Γ (low temperatures), while in the disordered system, $D(t)$ decreases over several orders of magnitude for large Γ. This behavior is reflected in the temperature dependence of the tracer correlation factor $f_{\rm tr}(\Gamma)=D_\infty/D_{\rm ST}$ shown in Fig. 2(c). In both the ordered and the disordered systems, $f_{\rm tr}$ is thermally activated,

$$f_{\rm tr}(\Gamma)=f_{\rm tr}(0)\exp(-\Delta E_f/k_BT)\ ,$$

but the activation energy ΔE_f, being the difference between the activation energies for the long- and short-time diffusion coefficients, is much larger in the disordered system ($\Delta E_f=0.05e^2/r_s=0.27V_0$) than in the ordered one ($\Delta E_f=0.01e^2/r_s=0.06V_0$). We conclude that, in order to obtain strong dispersion in the diffusive transport, we need both Coulomb interactions *and* structural disorder. In the following we will concentrate on this relevant case only and consider the curves shown in Fig. 2(b) in more detail.

For $\Gamma\ge 20$, an intermediate time regime $t_1<t<t_2$ occurs, where $D(t)$ shows approximate power-law behavior,

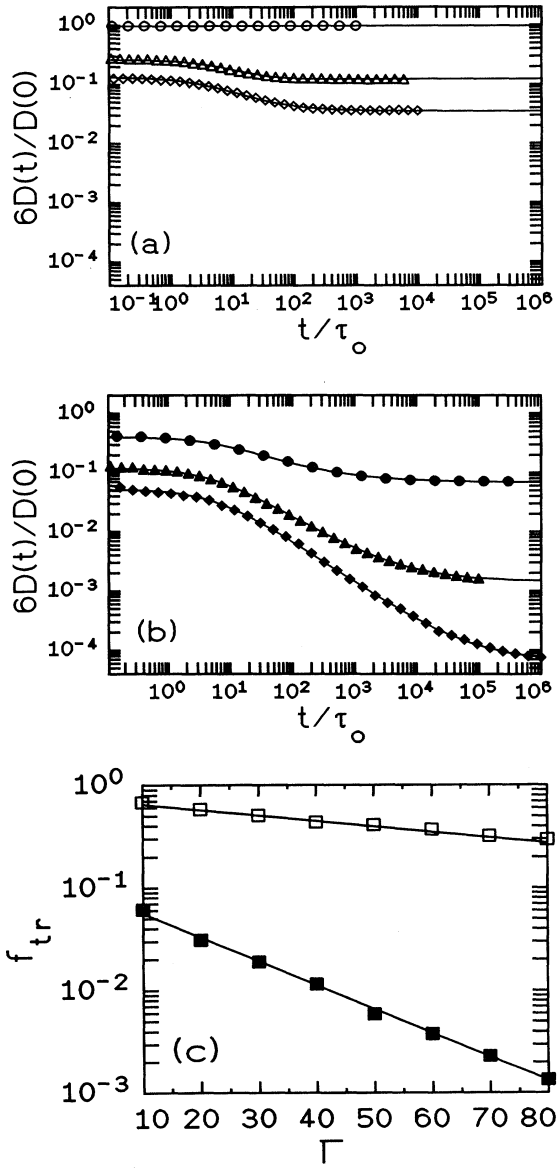

FIG. 2. Plot of (a) $D(t)$ in the ordered lattice for $\Gamma=0$ (○), 40 (△), and 80 (◇), (b) $D(t)$ in the disordered system for $\Gamma=0$ (●), 40 (▲), and 80 (◆), and (c) the tracer correlation factor as a function of the plasma parameter Γ in the ordered lattice (□) and in the disordered system (■). The full lines in (a) and (b) are least-square fits according to (17).

$$D(t)\sim t^{-n_D}, \quad t_1 < t < t_2 \ . \tag{16}$$

This time regime can be easily identified by drawing a straight line through the data points in the log-log plot. The upper crossover time t_2 and the exponent n_D increase with increasing Γ (decreasing temperature), while the lower crossover time t_1 is approximately independent of Γ and of the order of the inverse hopping rate $a^2/6D_{\rm ST}$. The whole time dependence of $D(t)$ can be well described by the formula

$$D(t)=D_\infty+(D_{\rm ST}-D_\infty)\left[1+\frac{t}{t_1}\right]^{-\tilde{n}_D}, \tag{17}$$

which has been suggested earlier by Funke on the basis of his jump relaxation model.[8]

Since the crossover regimes and the power-law regime are not fully separated except at very large plasma parameters, the exponent $\tilde{n}_D$ differs from the exponent n_D obtained from the "by hand" procedure. This is shown in Fig. 3, where $\tilde{n}_D$ and n_D are shown as functions of Γ. Both exponents increase with increasing Γ, but the dependence of n_D on Γ is more pronounced. At large plasma parameters where $t_2 \gg t_1$, the two exponents become the same.

From the Nernst-Einstein relation (6) we expect that the power-law behavior of $D(t)$ at intermediate time scales is reflected in a power-law behavior of $\hat{\sigma}(\omega)$ at intermediate-frequency scales, $1/t_2 < \omega < 1/t_1$. To determine $\hat{\sigma}(\omega)$ we have studied the current response to an external electric field $E(t)=E_0\sin(\omega t)$ as described in Sec. III. Figure 4 shows, as an example, the current density $J(t)$ in units of $J_0 \equiv e^2E_0/2k_BTa\tau_0$ as a function of ωt for $\Gamma=40$ and various frequencies in the three different frequency regimes (see Fig. 5) (a) the dc regime, (b) the dispersive regime, and (c) the high-frequency plateau. In both the dc and the high-frequency regimes $J(\omega t)$ does not change with frequency and there is no phase shift between the currents and the electric field. In the dispersive regime the amplitudes increase with frequency and the currents run ahead of the electric field.

Figure 5 shows the real and imaginary parts $\sigma'(\omega)$ and $\sigma''(\omega)$ of the conductivity $\hat{\sigma}(\omega)$ in units of $\sigma_0 \equiv e^2/2k_BTa\tau_0$ as a function of $\omega\tau_0$ for (a) $\Gamma=0$, (b) $\Gamma=40$, and (c) $\Gamma=80$. For comparison we show also the real and imaginary parts of $\hat{\sigma}_D(\omega)\equiv\rho e^2\hat{D}(\omega)/k_BT$ (full lines in the figure), which one obtains for the complex conductivity when neglecting the cross correlations in the autocorrelation function of the current density in Eq. (5). The frequency-dependent tracer diffusion coefficient $\hat{D}(\omega)$ is obtained numerically by a Laplace transform of $\langle r^2(t)\rangle$ [see Eq. (3)]. Since $\sigma''(\omega)\le 0$, we have plotted $-\sigma''(\omega)$ in the figure. For $\Gamma=0$, $\hat{\sigma}(\omega)$ and $\hat{\sigma}_D(\omega)$ coincide, since in this case the cross correlations practically vanish (the effect of the hard-core interaction between the mobile ions can be neglected since $\rho=0.01/a^3$ is very small). For $\Gamma=40$ and 80, $\hat{\sigma}(\omega)$ and $\hat{\sigma}_D(\omega)$ are equal at

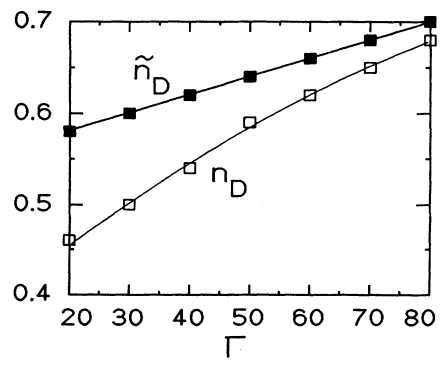

FIG. 3. Exponents n_D(□) and $\tilde{n}_D$ (■) as a function of Γ for $p=0.4$. The full lines are guides for the eye.

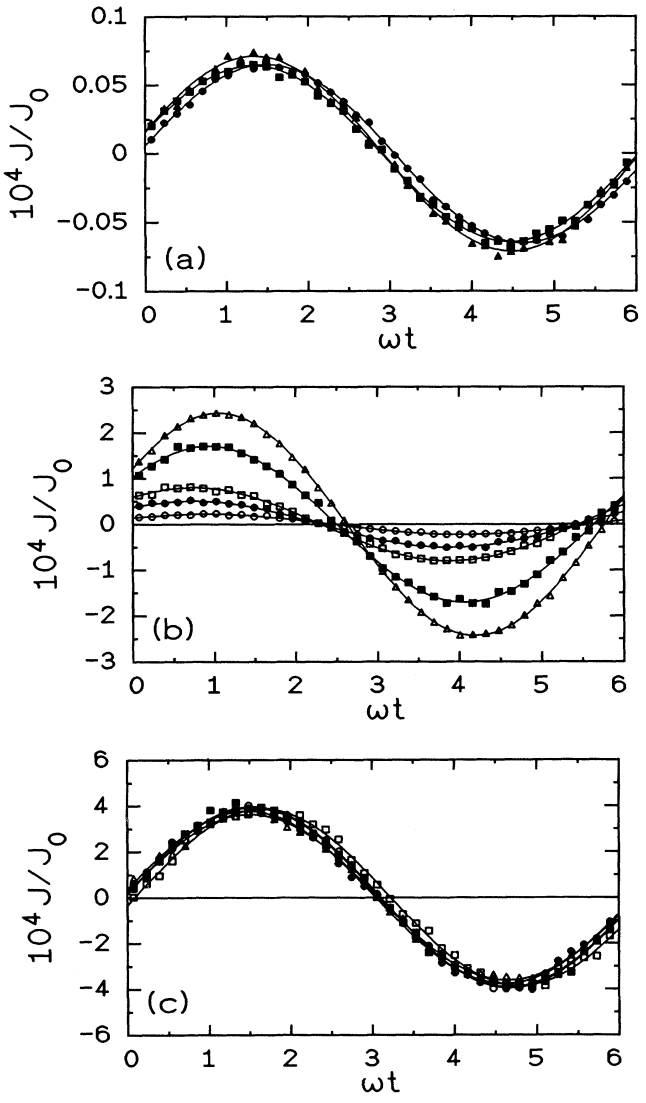

FIG. 4. Plot of the current density $J(t)$ in units of $J_0 \equiv e^2E_0/2k_BTa\tau_0$ as a function of time for $\Gamma=40, p=0.4$, and different frequencies in (a) the dc regime for $\omega\tau_0=1.3\times10^{-5}$ (■), 3.2×10^{-5} (●), and 5.0×10^{-5} (▲), (b) the dispersive regime for $\omega\tau_0=1.0\times10^{-3}$ (○), 4.0×10^{-3} (●), 1.0×10^{-2} (□), 4.0×10^{-2} (■), and 1.0×10^{-1} (△), and (c) the high-frequency plateau for $\omega\tau_0=4$ (○), 5 (●), 6.3 (□), 8.9 (■), and 10 (△).

high frequencies, but deviate at lower frequencies. Despite this, the overall behavior is quite similar. Both $\sigma'(\omega)$ and $\sigma'_D(\omega)$ exhibit a dc plateau at low frequencies $\omega \ll 1/t_2$ and approach $\sigma_\infty = \rho e^2 D_{ST}/k_B T$ at high frequencies $\omega \gg 1/t_1$. In between they can be approximately described by

$$\sigma'(\omega) \sim (\omega\tau_0)^{n_\sigma}, \quad \tau_0/t_2 \ll \omega\tau_0 \ll \tau_0/t_1 , \tag{18}$$

where $n_\sigma = n_D$. The crossover time t_2 can now be identified with the conductivity relaxation time τ_σ defined in Eq. (1). At very high frequencies the conductivity becomes constant again. However, at very large frequencies dynamical processes (vibrations of ions and counterions, etc.) not included in the lattice-gas model become dominant (see also Ref. 32) and the high-frequency plateau is difficult to detect experimentally (an exception is presented in Ref. 2).

The imaginary parts $\sigma''(\omega)$ and $\sigma''_D(\omega)$ show a minimum near $\omega\tau_0 \approx 10^{-1}$, where the phase shift between current and electric field is maximal. On the high-frequency side of the minimum, both curves become equal and decrease rapidly to zero. At the low-frequency side both curves show approximate power-law behavior, $\sigma''(\omega) \sim \sigma''_D(\omega) \sim (\omega\tau_0)^{n_\sigma}$.

Since $\tau_\sigma = t_2$ is the typical time scale for the conductivity relaxation, it is tempting to try if $\hat{\sigma}(\omega, T)$ can be described by the scaling ansatz

$$\frac{\hat{\sigma}(\omega, T)}{\hat{\sigma}(0, T)} = \hat{f}(\omega\tau_\sigma) , \tag{19}$$

where $\hat{f}(x) = 1$ for $x \ll 1$ and $\hat{f}(x) \sim (ix)^{n_\sigma}$ for $x \gg 1$ (the high-frequency plateau, which is seldom seen in experiments, is not of interest here). Figure 6 shows $\sigma'(\omega)$ as a function of $\omega\tau_\sigma$ for various plasma parameters Γ. The absence of a data collapse in Fig. 6 indicates that $\hat{\sigma}(\omega)$ obeys no simple scaling behavior. The inset of Fig. 6 demonstrates the absence of scaling also for the related quantity $D'(\omega)$. The reason for the absence of scaling is that the exponent n_σ (n_D) increases with decreasing temperature (see Fig. 3), and therefore the temperature dependence of σ cannot be described by changing the frequency scale alone.

For a quantitative analysis of the cross correlations we have determined the generalized frequency-dependent Haven ratio $\hat{H}_R(\omega)$ [see Eq. (7)]. Figure 7 shows the real and imaginary parts of $\hat{H}_R(\omega) = H'_R(\omega) + iH''_R(\omega)$ as a function of $\omega\tau_0$ for $\Gamma = 0$, 40, and 80. For $\Gamma = 0$, $\hat{H}_R(\omega) = 1$, since the cross correlations vanish. For $\Gamma = 40$ and 80, $H'_R(\omega)$ runs through a flat minimum near $\omega\tau_0 \simeq 10^{-2}$ and finally approaches the ordinary Haven ratio $H_R \simeq 0.8$ when ω moves into the dc regime. The imaginary part $H''_R(\omega)$ vanishes for large and small frequencies where the current is in phase with the applied

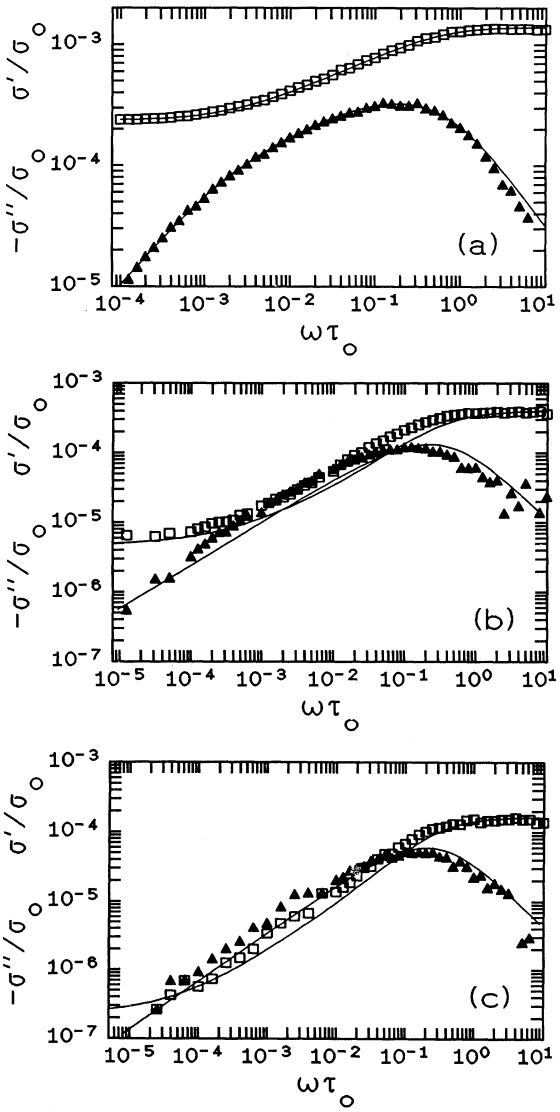

FIG. 5. Real (□) and imaginary parts (▲) of the conductivity for (a) $\Gamma = 0$, (b) $\Gamma = 40$, and (c) $\Gamma = 80$. The full lines are explained in the text.

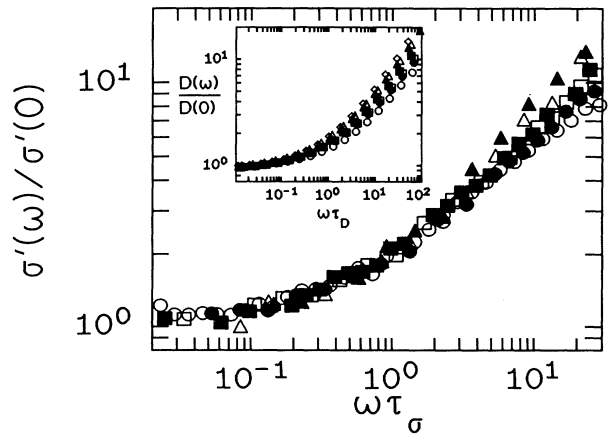

FIG. 6. Scale plot of $\sigma(\omega)/\sigma(0)$ versus $\omega\tau_\sigma$ for $p = 0.4$. The symbols refer to different plasma parameters $\Gamma = 10$ (○), 20 (●), 30 (□), 40 (■), 50 (△), and 60 (▲). The inset shows $D(\omega)/D(0)$ as a function of $\omega\tau_D$, for the same values of Γ.

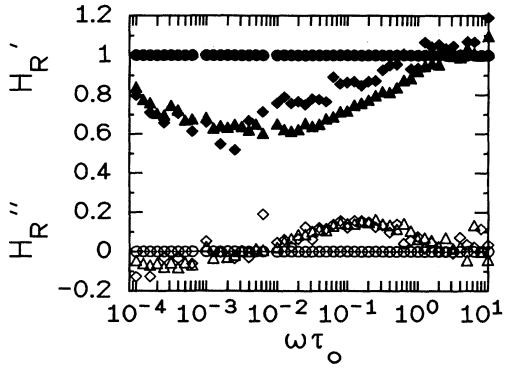

FIG. 7. Real (upper curves) and imaginary part (lower curves) of the generalized Haven ratio as a function of frequency. Different symbols refer to different plasma parameters, $\Gamma=0$ (○), 40 (◇), and 80 (△).

electric field, and goes through a flat maximum near $\omega\tau_0\approx 10^{-1}$. It is significant that the Haven ratio depends only weakly on ω or Γ. In contrast, as is demonstrated in Fig. 8 for $\omega=0$ and $\Gamma=30$, the Haven ratio depends considerably on the amount of disorder in the system, ranging from $\frac{1}{2}$ at $p=1$ to much higher values (around 0.8) at the percolation threshold ($p=0.312$), where the disorder is at its maximum. The increase of H_R with increasing disorder can be understood as follows: The blocked sites hinder the surrounding particles of the tracer particle from following it, and hence the cross correlations are diminished as the number of blocked sites is increased.

Since the cross correlations do not strongly affect the overall behavior of $\sigma(\omega)$ one can hope to understand the origin of the strong conductivity dispersion from the behavior of the time-dependent tracer diffusion coefficient. Indeed, to map the complex dynamics of the many-particle system to an effective dynamics of a one-particle system, it has been suggested that the mutual interactions between the ions can be described by an effective distribution $\psi(\tau_w)$ of waiting times τ_w between successive jumps of a tracer particle. This continuous-time random-walk (CTRW) model (see, e.g., Ref. 33) was proposed by Scher and Lax[34] to describe the dielectric response of amorphous semiconductors.

To test if the CTRW model applies here, we have determined the number $N(\tau_w)$ of waiting times τ_w' between two successive jumps of a tracer particle, which lie in the interval $\tau_w-\Delta\tau_w\le\tau_w'<\tau_w+\Delta\tau_w$. The waiting-time distribution $\psi(\tau_w)$ is related to $N(\tau_w)$ by $\psi(\tau_w)=AN(\tau_w)/2\Delta\tau_w$, where the prefactor A follows from the normalization condition, $\int_0^\infty d\tau_w\psi(\tau_w)=1$. Figure 9 shows $\psi(\tau_w)$ times τ_0 as a function of τ_w/τ_0 for various plasma parameters Γ. For all values of Γ, $\tau_0\psi(\tau_w)\simeq 10^{-1}$ is approximately constant for $\tau_w/\tau_0<1$ and decreases rapidly for $\tau_w/\tau_0>10$. As one would expect, the decrease is weaker for larger Γ, but no significant change of $\psi(\tau_w)$ occurs if Γ is increased.

The one-sided Fourier transform of the waiting-time distribution $\psi(\tau_w)$ is (within the CTRW model) related to the frequency-dependent diffusion coefficient $\hat{D}_w(\omega)$ by[34]

$$\hat{D}_w(\omega)=\frac{a^2}{6}\frac{i\omega\hat{\psi}(\omega)}{1-\hat{\psi}(\omega)} . \tag{20}$$

In Fig. 10 we compare $D_w'(\omega)/D_0$ [obtained from (20)] with the correct $D'(\omega)/D_0$ [obtained from (3)] for $\Gamma=80$. The two curves are completely different: In contrast to $D'(\omega)$, $D_w'(\omega)$ shows only a very little dispersion. The *low*-frequency limit of $D_w'(\omega)$ is the same as the *high*-frequency limit of $D'(\omega)$.

These deviations show clearly the principal difficulties of the CTRW model (see also Ref. 35). If the initial waiting time τ_w^0 that the tracer particle needs for the first jump is chosen according to the proper *stationary distribution,*

$$\psi_0(\tau_w^0)=\int_0^\infty d\tau_w\psi(\tau_w^0+\tau_w)/\int_0^\infty d\tau_w^0\int_0^\infty d\tau_w\psi(\tau_w^0+\tau_w) ,$$

$D(\omega)$ shows no dispersion at all, $D(\omega)=D_{ST}$ just as in the simple random-walk case. The larger value of D_w at high frequencies is an artifact of the CTRW model and results from the fact that the initial time τ_w^0 is assumed to be distributed according to ψ rather than to the stationary distribution.

Since the time inhomogeneities in the tracer motion

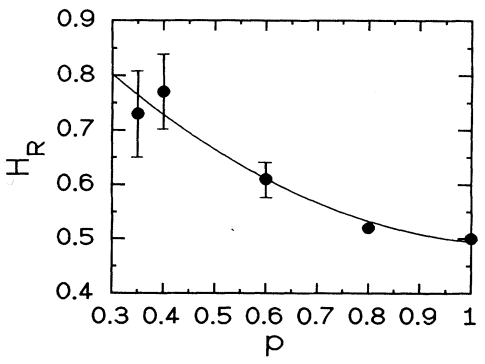

FIG. 8. Haven ratio as a function of the disorder parameter p for $\omega=0$ and $\Gamma=30$.

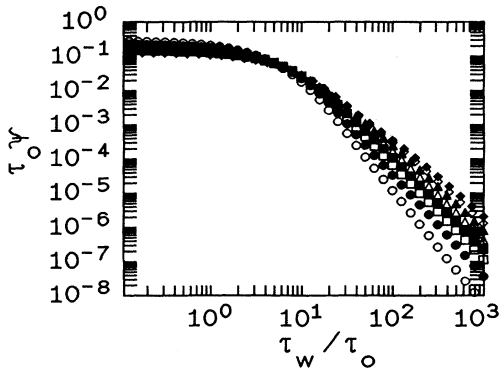

FIG. 9. Plot of the distribution function of the waiting time τ_w between successive jumps as a function of τ_w/τ_0 for different plasma parameters $\Gamma=10$ (○), 20 (●), 30 (■), 40 (■), 50 (△), 60 (▲), 70 (◇), and 80 (◆).

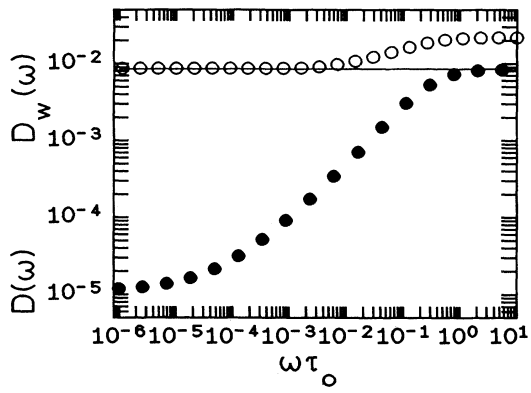

FIG. 10. Comparison of the real part of the diffusion coefficient $D'_w(\omega)/D_0$ [obtained from the approximation (22)] (○) and the correct $D'(\omega)/D_0$ [obtained from (3)] (●) for $\Gamma=80$.

cannot be responsible for the dispersion, we now study spatial correlations in the tracer trajectory. We consider the mean square displacement $\langle r^2(N_{\rm hop})\rangle$ as a function of the number of performed hops $N_{\rm hop}$, which is shown in Fig. 11 for various plasma parameters Γ. At $N_{\rm hop}=1$, $\langle r^2(N_{\rm hop})\rangle/a^2=1$ for all Γ since a tracer particle has moved the distance a after the first jump. At small plasma parameters, $\langle r^2(N_{\rm hop})\rangle$ increases monotonically with $N_{\rm hop}$. At larger values of $\Gamma(\Gamma\geq 20)$, a striking alternation of $\langle r^2(N_{\rm hop})\rangle$ for even and odd $N_{\rm hop}$ begins to emerge for $1<N_{\rm hop}<N_{\rm hop}^{(2)}$, which becomes more pronounced at larger Γ. The upper crossover number $N_{\rm hop}^{(2)}$ increases with increasing Γ and is of the order of the product of the jump rate $6D_{\rm ST}/a^2$ and the crossover time $t_2\approx\tau_\sigma$, $N_{\rm hop}^{(2)}\simeq 6D_{\rm ST}t_2/a^2$. For even values of $N_{\rm hop}$, $\langle r^2(N_{\rm hop})\rangle$ shows approximate power-law behavior,

$$\langle r^2(2N_{\rm hop})\rangle\sim(2N_{\rm hop})^k,\quad 1<N_{\rm hop}<N_{\rm hop}^{(2)}\ , \tag{21}$$

where $k=1-n_D=1-n_\sigma$ is the exponent expected from the behavior of $\langle r^2(t)\rangle$, if t is simply replaced by the average time $2N_{\rm hop}a^2/6D_{\rm ST}$ after $2N_{\rm hop}$ jumps of the tracer particle,

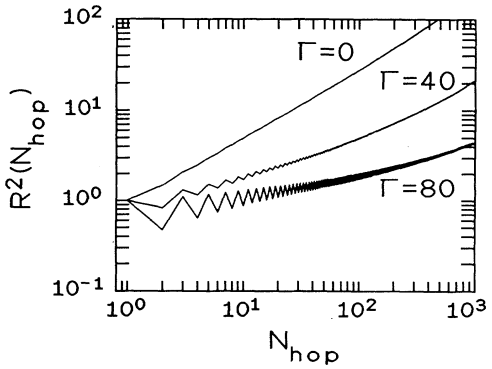

FIG. 11. Mean-square displacement $\langle r^2(N_{\rm hop})\rangle$ as a function of the number of performed hops $N_{\rm hop}$ for different plasma parameters Γ.

$$\langle r^2(2N_{\rm hop})\rangle\simeq\langle r^2(t=2N_{\rm hop}a^2/6D_{\rm ST})\rangle\ .$$

The striking alternation of $\langle r^2(N_{\rm hop})\rangle$ is caused by strong forward-backward correlations in the tracer motion, which occur on length scales of the order of the lattice constant a. Before its first jump the tracer ion finds itself in a deep energy minimum, which is created by the surrounding ions. After its first jump the ion is in an energetically unfavorable situation and has a large tendency to jump back to the original site. Thus

$$\langle r^2(N_{\rm hop}=2)\rangle<\langle r^2(N_{\rm hop}=1)\rangle=a^2\ .$$

Repetition of these forward-backward jumps leads to the alternating behavior of $\langle r^2(N_{\rm hop})\rangle$. Sometimes it happens that an energetically unfavorable position is stabilized by jump relaxation processes of the surrounding ions. This causes $\langle r^2(N_{\rm hop})\rangle$ to increase slightly, but the increase is much weaker than in the absence of the forward-backward correlations. The presence of disorder is important for the forward-backward correlations to arise because the surrounding ions cannot follow the tracer ion without making detours, which delays the local relaxation process considerably. A similar suppression of the mobility of the surrounding ion cloud can be expected to occur in ordered lattices by a complex lattice structure with several sites per unit cell, as, for example, in the crystalline superionic conductor $RbAg_4I_5$. In ordered Bravais lattices, the surrounding ions can easily stabilize the position of the tracer ion and the forward-backward correlations are very small. The forward-backward correlations dominate the overall behavior on the length scale of the lattice constant. When $\langle r^2(N_{\rm hop})\rangle^{1/2}$ has reached a few lattice constants at $N_{\rm hop}\gg N_{\rm hop}^{(2)}$, the effect ceases to be dominant and the dispersion becomes considerably weaker.

In order to understand why the even values of $N_{\rm hop}$ between 1 and $N_{\rm hop}^{(2)}$ determine the behavior of $\langle r^2(t)\rangle$ between $t_1\simeq a^2/6D_{\rm ST}$ and $t_2\simeq N_{\rm hop}^{(2)}a^2/6D_{\rm ST}$, one must be aware that for a fixed time t the probability that the tracer ion has performed an even number of jumps is much larger than the probability that it has performed an odd number of jumps. After an odd number of jumps the tracer ion mostly finds itself in an energetically unfavorable position and stays there only for a short time (compared to the time spent on a site after an even number of jumps). Hence the probability that a particle has performed an odd number of jumps at a given time t is small, and does not contribute to the mean square displacement at t.

The forward-backward correlations also cause characteristic changes of the distribution function $P(\mathbf{r},t)$ and its Fourier transforms. Figure 12(a) shows $\log_{10}[P(\mathbf{r},t)/P(0,t)]$ as a function of the scaled distance $r/R(t)$, where $R(t)=\langle r^2(t)\rangle^{1/2}$ is the root mean square displacement, in the disordered system for $\Gamma=40$ and 80 and several times t in the dispersive regime. It is remarkable that, although $R(t)$ is small in this regime, the curves collapse, showing that the simple scaling relation $P(\mathbf{r},t)/P(0,t)=f(r/R(t))$ holds as in the simple random-walk case. For $\Gamma=40$ and 80, the scaling function $f(x)$ is no longer a Gaussian, but a stretched Gauss-

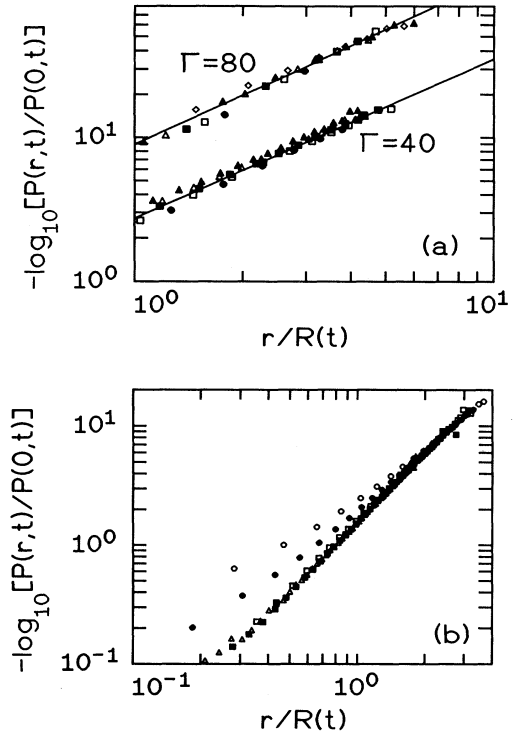

FIG. 12. Scale plot of the distribution function $\log_{10}[P(\mathbf{r},t)/P(0,t)]$ versus $r/R(t)$ in the disordered system ($p=0.4$) for (a) $\Gamma=40$ and 80 and (b) $\Gamma=0$. Different symbols refer to different times. In (a) for $\Gamma=40, t/\tau_0=546$ (●), 1130 (□), 2340 (■), 4830 (△), and 10 000 (▲), and for $\Gamma=80, t/\tau_0=113$ (●), 264 (□), 616 (■), 1440 (△), 3360 (▲), and 7850 (◇); in (b) $t/\tau_0=3231$ (○), 8000 (●), 19 800 (□), 49 000 (■), and 121 000 (△). The curve for $\Gamma=80$ in (a) has been multiplied by a factor of 2.

ian, $f(x)=\exp(-cx^u)$, with $u\simeq 1.2$. For $\Gamma=0$ in contrast, $P(\mathbf{r},t)$ shows the expected scaling behavior with a Gaussian scaling function only at larger times [Fig. 12(b)]. It is interesting to note that the exponent u satisfies the relation

$$u=\frac{2}{1+\tilde{n}_D}\ , \tag{22}$$

which was originally derived to describe the distribution function of random walks on random fractal structures.[36]

In order to discuss the Fourier transform of $P(\mathbf{r},t)$, the intermediate scattering function, we first remove any artificial effects of the lattice anisotropy by averaging $S_{\rm inc}(\mathbf{k},t)$ over the angle distribution

$$\tilde{S}_{\rm inc}(k,t)\equiv(4\pi)^{-1}\int d\Omega\, S_{\rm inc}(\mathbf{k},t)\ .$$

For $kR(t)\ll 1$ and $R(t)\ll 1$ it is easy to verify that $\tilde{S}_{\rm inc}(k,t)$ can be approximated by

$$\tilde{S}_{\rm inc}(k,t)\simeq\exp\left[-\frac{k^2R^2(t)}{6}\right]\ . \tag{23}$$

Figure 13 shows $1-\tilde{S}_{\rm inc}(k,t)$ for $k=2\pi/10a$ and $\Gamma=0$, 40, and 80. Quite surprisingly, the simple approximation

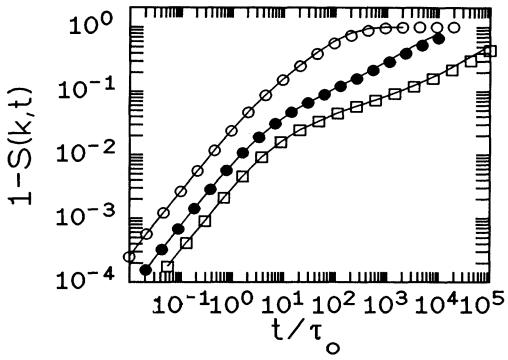

FIG. 13. Plot of $1-\tilde{S}_{\rm inc}(k,t)$ for $k=2\pi/10a$ and $\Gamma=0$ (○), 40 (●), and 80 (□). The full lines are the approximation (23).

(23) holds in the whole decay regime, showing that the decay changes from a simple to a stretched exponential when Γ becomes larger (see also Ref. 8).

Next we discuss the NMR correlation functions $G^{(q)}(t)$, $q=1,2$. We again compare our results for the ordered lattice ($p=1$) and the disordered substrate ($p=0.4$). For sufficiently large values of $\Gamma(\Gamma>1)$ the distribution of the mobile ions is isotropic and therefore $G^{(2)}(0)=4G^{(1)}(0)$.[25] Numerically we find that for $\Gamma>10$, $G^{(2)}(t)\cong 4G^{(1)}(t)$ is valid for all times t, and thus

$$G^{(2)}(t)/G^{(2)}(0)\equiv G^{(1)}(t)/G^{(1)}(0)\ .$$

Since the $G^{(q)}(t)$ decay faster than $1/t$ for very long times, the asymptotics is irrelevant for $1/T_1$ (see the discussion above, Sec. II D), and the relevant decay regime is most conveniently discussed in terms of the functions $1-G^{(q)}(t)/G^{(q)}(0)$, which are shown in Fig. 1(a) in Ref. 18. Both in the ordered lattice and the disordered system, $1-G^{(q)}(t)/G^{(q)}(0)$ are proportional to t/τ_0 for small t/τ_0 values. As in the diffusion constant, an intermediate time regime can be well identified in the disordered system for $\Gamma>20$, where

$$1-G^{(q)}(t)/G^{(q)}(0)\sim(t/\tau_0)^{1-n_{\rm NMR}}\ .$$

The exponent $n_{\rm NMR}$ is independent of temperature, $n_{\rm NMR}\cong 0.73$. In the ordered lattice, the decay of the $G^{(q)}(t)$ is much faster and a corresponding intermediate time interval is hardly seen. We define $\tau_{\rm NMR}$ as the time where $G^{(q)}(t)$ has decreased to $1/e$ of its initial value, $G^{(q)}(\tau_{\rm NMR})/G^{(q)}(0)=1/e$. We found that, due to strong correlations in the ionic motion, $\tau_{\rm NMR}$ is more strongly activated than τ_0, $\tau_{\rm NMR}/\tau_0=\exp(\Delta E_{\rm NMR}/k_BT)$, $\Delta E_{\rm NMR}\equiv E_{\rm NMR}-V_0>0$. The activation energy $\Delta E_{\rm NMR}$ is smaller in the ordered lattice,

$$\Delta E_{\rm NMR}\cong 0.04e^2/r_s=(0.04\eta V_0)\ ,$$

than in the disordered system,

$$\Delta E_{\rm NMR}\cong 0.09e^2/r_s=(0.09\eta V_0)\ ,$$

where $\tau_{\rm NMR}$ exceeds τ_0 by more than five orders of magnitude for $\Gamma=80$. Closer inspection shows that, on time scales larger than τ_0, $G^{(q)}(t)/G^{(q)}(0)$ is only a function of

$t/\tau_{\rm NMR}$ (independent of Γ); in particular,

$$1-G^{(q)}(t)/G^{(q)}(0)\sim(t/\tau_{\rm NMR})^{1-n_{\rm NMR}}$$

for $\tau_0/\tau_{\rm NMR}\ll t/\tau_{\rm NMR}<1$ [see Fig. 1(b) in Ref. 18]. Accordingly, the correlation functions can be written approximately in Kohlrausch-Williams-Watts (KWW) form,

$$G^{(q)}(t)=G^{(q)}(0)\exp[-(t/\tau_{\rm NMR})^{1-n_{\rm NMR}}],$$

in the relevant decay regime.

From Eq. (11) we obtain $1/T_1(\omega,T)$ by Fourier transformation. Figure 14 shows $1/T_1(\omega,T)$ as a function of V_0/k_BT for $\eta=5$ and various Larmor frequencies ω in (a) the ordered lattice, and (b) the disordered system. For comparison, we show in (c) also the behavior of $1/T_1$ for uncharged particles ($\eta=0$, $\Gamma\equiv0$) diffusing in the disordered system. Since in all cases (a)–(c) the $G^{(q)}(t)$ decay faster than $1/t$ for large times, $1/T_1$ is independent of ω at the high-temperature side of the maximum. For the uncharged particles [Fig. 14(c)], $1/T_1$ shows no significant deviation from the standard BPP behavior. For charged particles slight deviations occur in the ordered lattice [Fig. 14(a)], but the typical non-BPP behavior according to Eq. (2) does not occur. The deviations predominantly show up in a weak asymmetry of $1/T_1$ near the maximum. In case (b), when both disorder and Coulomb interactions are present, we obtain the typical non-BPP behavior: The curves are asymmetric in shape, the maximum occurs at $\omega\tau_{\rm NMR}\approx1\gg\omega\tau_0$, and $1/T_1$ decreases as $1/T_1\sim\tau_0(\omega\tau_0)^{n_{\rm NMR}-2}$ at low temperatures ($\omega\gg1/\tau_{\rm NMR}$). The activation energies are $E_1^{\rm NMR}\cong1.5V_0$ and $E_2^{\rm NMR}\cong0.4V_0$. Note that $E_{\rm NMR}\cong1.45V_0$ for $\eta=5$ (see above) and thus $E_{\rm NMR}\simeq E_1^{\rm NMR}$. We conclude that, similarly to our result for the conductivity $\sigma(\omega)$, both structural disorder and Coulomb interactions are needed to obtain qualitative agreement with the experimental findings. Again, we concentrate on this relevant case only.

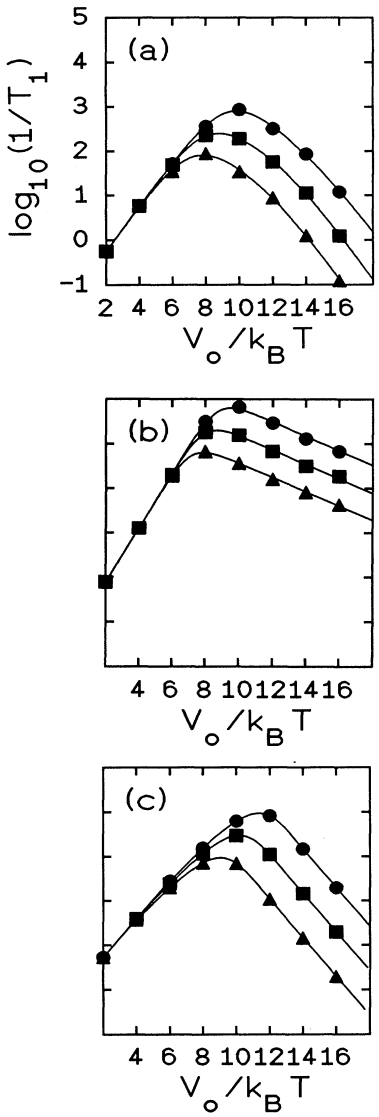

FIG. 14. Spin-lattice relaxation rate $1/T_1$ in units of $C\tau_\infty$ as a function of V_0/k_BT for $\eta=5$ (a) in the ordered lattice and (b) in the disordered system. For comparison (c) shows the case $\eta=5$ ($\Gamma\equiv0$) in the disordered system. Different symbols refer to different Larmor frequencies: in (a) $\omega\tau_\infty=3\times10^{-9}$ (●), 9.5×10^{-9} (■), and 3×10^{-8} (▲), in (b) $\omega\tau_\infty=3\times10^{-7}$ (●), 9.5×10^{-7} (■), and 3×10^{-6} (▲), and in (c) $\omega\tau_\infty=3\times10^{-6}$ (●), 9.5×10^{-6} (■), and 3×10^{-5} (▲).

As a consequence of the scaling behavior of $G^{(q)}(t)$, $1/T_1(\omega,T)$ obeys the simple scaling relation [see Fig. 3(a) in Ref. 18]

$$\frac{1}{T_1}(\omega,T)=\tau_{\rm NMR}g(\omega\tau_{\rm NMR}), \tag{24}$$

with $g(x)=$const for $x\ll1$ and $g(x)\propto x^{n_{\rm NMR}-2}$ for $x\gg1$. Equation (24) implies $E_1^{\rm NMR}=E_{\rm NMR}$ and the relation $E_2^{\rm NMR}=(1-n_{\rm NMR})E_1^{NMR}$ proposed by Ngai.[19]

Since $1/T_1(\omega,T)$ shows scaling behavior in contrast to $\sigma(\omega,T)$, it is clear that in general a simple relation between the two quantities, as suggested earlier,[8] does not exist. The difference between spin-lattice relaxation and conductivity is best demonstrated by comparison of the exponents n_σ and $n_{\rm NMR}$ and the crossover times τ_σ and $\tau_{\rm NMR}$, which are shown in Fig. 15 as functions of V_0/k_BT. This figure is very similar to Fig. 4 in Ref. 18, where the data for τ_σ were calculated from $D(\omega)$, showing again the minor importance of cross terms in the current correlation function.

As can be seen from the figure, n_σ is smaller than $n_{\rm NMR}$ for $V_0/k_BT<16$ and seems to approach $n_{\rm NMR}$ at lower temperatures. Only at these very low temperatures do we expect mean-field approaches[8] yielding $n_\sigma=n_{\rm NMR}$ to be applicable. From Fig. 15(b) we find that the conductivity relaxation time τ_σ is less activated than the NMR relaxation time $\tau_{\rm NMR}$, and therefore $\tau_{\rm NMR}/\tau_\sigma\gg1$ at lower temperatures. This is in accordance with very recent experimental results for $(LiCl)_{0.6}(Li_2O)_{0.7}(B_2O_3)_{1.0}$,[37] glassy $Li_2AlSi_2O_6$,[38] and fluorozirconate glasses.[6] The reason for these differences is that, although the phenomena observed in both experiments originate from the same ion transport mechanism,

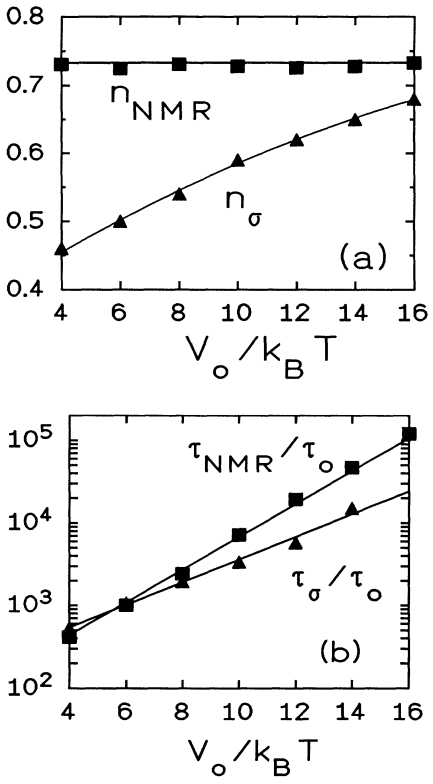

FIG. 15. (a) The exponents n_{NMR} and n_σ and (b) the relaxation times $\tau_{\mathrm{NMR}}/\tau_0$ and τ_σ/τ_0 as a function of V_0/k_BT in the disordered system.

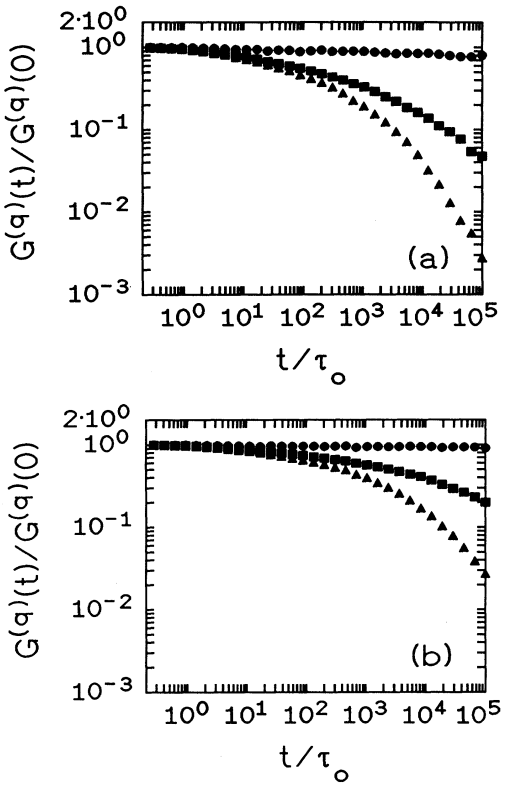

FIG. 16. The normalized correlation functions $G^{(q)}(t)/G^{(q)}(0)$ as functions of t/τ_0 for (a) $\Gamma=10$ and (b) $\Gamma=20$ and $p=0.312\cong p_c$ (●), 0.33 (■), and 0.35 (▲).

they are governed by *different* correlation functions: In spin-lattice relaxation (SLR), the correlation functions are determined by diffusion of ion pairs, while in conductivity the current correlation function is mainly determined by the diffusion of single ions.

Figure 15 has been obtained for "weak" disorder, where p was considerably larger than the percolation threshold $p_c\cong0.312$. It is interesting to note that near the percolation threshold the differences between spin-lattice relaxation and conductivity become much more pronounced (see also Ref. 39). Figure 16 shows $G^{(q)}(t)/G^{(q)}(0)$ versus t/τ_0 for $p=0.35$, 0.33, and $0.312\cong p_c$, and (a) $\Gamma=10$ and (b) $\Gamma=20$. When approaching p_c, the decay of the $G^{(q)}(t)$ is drastically slowed down, even for comparatively small values of the plasma parameter, and the typical decay time τ_{NMR} seems to diverge. Also the value of n_{NMR} increases considerably. In contrast, the intermediate-time behavior of $\langle r^2(t)\rangle$ remains nearly unchanged when approaching p_c. The reason for this spectacular behavior of $G^{(q)}(t)$ is that near the percolation threshold large regions of the system are not available for the ions. These regions are effectively oppositely charged and attract a fraction of the mobile ions to their boundaries. Due to the strong electric fields at the rough edges of the unavailable regions these screening ions have a very small mobility and a mutual distance that is less than the mean distance between all ions. Since in SLR short distances are weighted highly, the fraction of screening ions contributes strongly to the SLR correlation functions and dominates their behavior. In contrast, in the mean square displacement the mobile ions are the dominant ones, and the formation of ion complexes with a very small mobility leads only to a slight reduction of the hopping rate. We suggest that the drastic slowing down of the decay of the NMR correlation functions should be looked for in highly porous media where also an anomalous magnetic field dependence of $1/T_1$ at the high-temperature side of its maximum might occur.

V. CONCLUSIONS

In the present paper, we have studied a model for ionic transport in disordered systems, which keeps the essential physics (Coulombic interaction between the ions and blocking effects by structural disorder) but is simple enough to be treated numerically by Monte Carlo simulation techniques. For modeling the structural disorder, we have employed standard site percolation. We discussed several ionic transport quantities, such as the mean square displacement, the frequency-dependent conductivity, and the spin-lattice relaxation rate, and have shown that *both* ingredients (structural disorder *and* Coulomb interactions) are needed to find the typical dispersion behavior widely observed in experiments. It is remarkable that the simple model also shows the delicate differences between conductivity relaxation and spin-lattice relaxation found in recent experiments.

While the model describes well the dispersive transport behavior, it does not aim to explain all transport anomalies occurring in glasses or solid electrolytes, such as the mixed-alkali effect or the drastic increase of the dc conductivity with the ionic content found in ionic glasses (see, e.g., Ref. 40). For a description of these effects, the couplings of the mobile ions to the underlying structural network (including the background charges that here have been considered as homogeneously distributed) must be considered explicitly,[41–43] which was beyond the scope of the present work.

ACKNOWLEDGMENTS

We would like to thank W. Dieterich, K. Funke, P. Heitjans, M. D. Ingram, O. Kanert, and K. L. Ngai for many helpful discussions. We thank the Deutsche Forschungsgemeinschaft for financial support.

APPENDIX

The NMR correlation functions $G^{(q)}(t)$ defined in Eq. (13) can be expressed by the conditional probability $W(\mathbf{r}',t|\mathbf{r},0)$ to find two marked particles at distance $\mathbf{r}'$ at time t, if they had the distance $\mathbf{r}$ at time 0:

$$G^{(q)}(t)=\rho\int_{r,r'\geq a} d\mathbf{r}\,d\mathbf{r}'g(\mathbf{r})W(\mathbf{r}',t|\mathbf{r},0) \times F^{(q)*}(\mathbf{r}')F^{(q)}(\mathbf{r}) , \tag{A1}$$

where $g(\mathbf{r})$ is the static pair correlation function. For particles without interaction, $W(\mathbf{r}',t|\mathbf{r},0)$ can be written as the product of the probability $P(\mathbf{x},t)$ that one of the two particles has moved a distance $\mathbf{x}$ during time t and the probability $P(\mathbf{r}'-\mathbf{r}+\mathbf{x},t)$ that the other particle has moved a distance $(\mathbf{r}'-\mathbf{r}+\mathbf{x})$, averaged over all vectors $\mathbf{x}$,

$$W(\mathbf{r}',t|\mathbf{r},0)=\int d\mathbf{x}\,P(\mathbf{r}'-\mathbf{r}+\mathbf{x},t)P(\mathbf{x},t) . \tag{A2}$$

To determine the asymptotic time dependence of $G^{(q)}(t)$, we use the fact that $P(\mathbf{r},t)$ can be written as[28]

$$P(\mathbf{r},t)\sim R(t)^{-d}h(r/R(t)) , \tag{A3}$$

where $R(t)\equiv\langle r^2(t)\rangle^{1/2}$ is the root mean square displacement. After the convenient substitution $(\mathbf{r},\mathbf{r}',\mathbf{x}) \rightarrow (R(t)\mathbf{r},R(t)\mathbf{r}',R(t)\mathbf{x})$ we obtain from Eqs. (A1) and (A2)

$$G^{(q)}(t)\sim\rho R(t)^{d-6}\zeta^{(q)}(t) , \tag{A4}$$

where

$$\zeta^{(q)}(t)\equiv\int_{r,r'\geq a/R(t)} d\mathbf{r}\,d\mathbf{r}'g(R(t)\mathbf{r})h_2(\mathbf{r}'-\mathbf{r}) \times F^{(q)*}(\mathbf{r}')F^{(q)}(\mathbf{r}) \tag{A5}$$

and h_2 is the convolution of h with itself,

$$h_2(\mathbf{r}'-\mathbf{r})\equiv\int d\mathbf{x}\,h(\mathbf{r}'-\mathbf{r}-\mathbf{x})h(\mathbf{x}) . \tag{A6}$$

In an ordered lattice $g(R(t)\mathbf{r})=1$ for $r\geq a/R(t)$ and $R(t)=(a^2t/2d\tau_0)^{1/2}$. Assuming that $h_2(\mathbf{r}'-\mathbf{r})$ has a simple quadratic maximum for small $|\mathbf{r}'-\mathbf{r}|$, $h_2(\mathbf{r}'-\mathbf{r})\simeq c_1+c_2(\mathbf{r}'-\mathbf{r})^2$, it is easy to show that in $d=3$

$$\zeta^{(q)}(t)\sim\bar{c}_1-\bar{c}_2R(t)^{-1}=\bar{c}_1-\bar{c}_2t^{-1/2} .$$

In $d=2$, we have $\zeta^{(1)}(t)\sim$const and $\zeta^{(2)}(t)\sim R(t)^2\sim t$. In the special case where the applied field H is perpendicular to the substrate, $\zeta^{(1)}\equiv 0$.

Accordingly, $G^{(1)}(t)$ and $G^{(2)}(t)$ have the following asymptotic time dependence,

$$G^{(1)}(t)\sim\begin{cases} t^{-3/2}, & d=3, \\ t^{-1}, & d=2,\ B_\parallel\neq 0, \\ 0, & d=2,\ B_\parallel=0, \end{cases}$$
$$G^{(2)}(t)\sim\begin{cases} t^{-3/2}, & d=3, \\ t^{-2}, & d=2,\ B_\parallel\neq 0, \\ t^{-2}, & d=2,\ B_\parallel=0, \end{cases} \tag{A7}$$

where $B_\parallel$ is the magnetic field component parallel to the substrate in the two-dimensional case.

The power-law decay of $G^{(q)}(t)$ at large times is demonstrated in Fig. 17(a) for $d=3$, where we show the result for $G^{(q)}(t)/G^{(q)}(0)$ of our numerical simulation. The corresponding exponential decay of the BPP ansatz is also shown for comparison. Although the correct

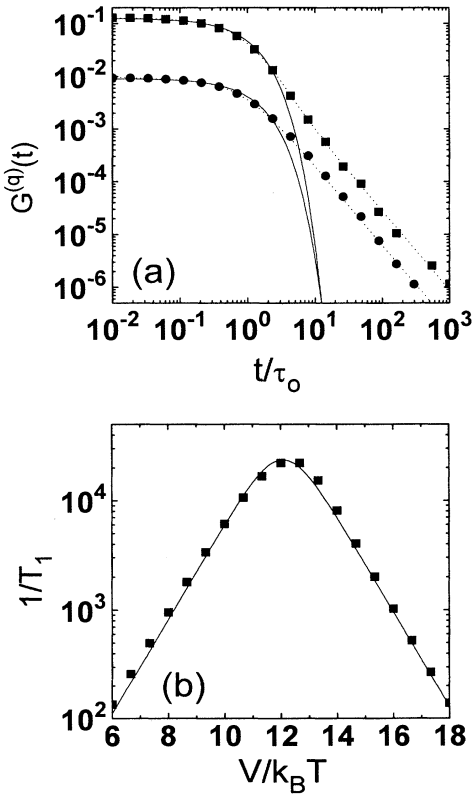

FIG. 17. (a) NMR correlation functions $G^{(1)}(t)$ (●) and $G^{(2)}(t)$ (■) for a simple random walk ($\eta=0,\Gamma\equiv 0$) in a sc lattice as a function of t/τ_0 and (b) the spin-lattice relaxation rate $1/T_1$ as a function of V_0/k_BT. The full lines in (a) and (b) show the results of the BPP ansatz. The dotted lines in (a) are guides for the eye.

curves and those of the BPP ansatz differ strongly for $t/\tau_0 \gg 1$, the spin-lattice relaxation rate is approximately the same in both cases [see Fig. 17(b)]. This is due to the fact that in both cases the correlation functions $G^{(q)}(t)$ decrease linearly with time for short times $t/\tau_0 \ll 1$ and faster than t^{-1} for large times. Accordingly, we have [see Eqs. (11) and (12)], $1/T_1 \sim \tau_0(\omega\tau_0)^{-2}$ for $\omega\tau_0 \gg 1$ and $1/T_1 \sim \tau_0$ independent of frequency for $\omega\tau_0 \ll 1$. In the two-dimensional case, a logarithmic dependence of $1/T_1$ on the magnetic field is expected to occur on the high-temperature side of the $1/T_1$ maximum ($\omega\tau_0 \ll 1$) as long as the magnetic field has a component parallel to the substrate. Recently, this logarithmic field dependence has been observed very nicely in $Li_{0.7}TiS_2$.[44]

*Present address: Department of Physics, University of California, Los Angeles, California 90024.

[1]H. Jain, N. L. Peterson, and H. L. Downing, J. Non-Cryst. Solids **55**, 283 (1983).
[2]K. Funke, Prog. Solid State Chem. **22**, 111 (1993).
[3]C. T. Moynihan, L. P. Boesch, and N. L. Laberge, Phys. Chem. Glasses **14**, 122 (1973).
[4]M. D. Ingram, Phys. Chem. Glasses **28**, 215 (1987).
[5]O. Kanert, J. Steinert, H. Jain, and K. L. Ngai, J. Non-Cryst. Solids **131-133**, 1001 (1991); O. Kanert, R. Küchler, K. L. Ngai, and H. Jain, Phys. Rev. B **49**, 76 (1994).
[6]O. Kanert, R. Küchler, J. Diekhöfer, X. Lu, and H. Jain, Phys. Rev. B **49**, 629 (1994).
[7]P. Heitjans, W. Faber, and A. Schirmer, J. Non-Cryst. Solids **131-133**, 1053 (1991); P. Heitjans, Solid State Ionics **18/19**, 50 (1986); W. Franke and P. Heitjans, Ber. Bunsenges. Phys. Chem. **96**, 1674 (1992).
[8]K. Funke and I. Riess, Z. Phys. Chem. Neue Folge **140**, 217 (1984); K. Funke, *ibid.* **154**, 251 (1987).
[9]T. Suemoto and M. Ishigame, Phys. Rev. B **33**, 2757 (1986).
[10]L. Börjesson, L. M. Torrel, and W. S. Howells, Philos. Mag. B **59**, 105 (1989); L. Börjesson, Phys. Rev. B **36**, 4600 (1987).
[11]G. Carini, M. Federico, and G. Tripodo, Philos. Mag. B **65**, 153 (1992).
[12]D. P. Almond, G. K. Duncan, and A. R. West, Solid State Ionics **8**, 159 (1983).
[13]A. K. Jonscher, Nature **267**, 673 (1977).
[14]S. H. Chung, K. R. Jeffrey, J. R. Stevens, and L. Börjesson, Phys. Rev. B **41**, 6154 (1990).
[15]N. Bloembergen, E. M. Purcell, and R. V. Pound, Phys. Rev. **73**, 679 (1948).
[16]A. Bunde, D. K. Chaturvedi, and W. Dieterich, Z. Phys. B **47**, 209 (1982); A. Bunde and W. Dieterich, Phys. Rev. B **31**, 6012 (1985).
[17]P. Maass, J. Petersen, A. Bunde, W. Dieterich, and H. E. Roman, Phys. Rev. Lett. **66**, 52 (1991).
[18]M. Meyer, P. Maass, and A. Bunde, Phys. Rev. Lett. **71**, 573 (1993).
[19]K. L. Ngai, Comments Solid State Phys. **9**, 127 (1979); **9**, 141 (1979); in *Fast Ion Transport in Solids*, edited by P. Vashishta, J. N. Mundy, and G. K. Shenoy (North-Holland, New York, 1979); K. L. Ngai and O. Kanert, Solid State Ionics **53-56**, 936 (1992).
[20]S. R. Elliott and A. P. Owens, Phys. Rev. B **44**, 47 (1991).
[21]W. Schirmacher, M. Prem, J.-B. Suck, and A. Heidemann, Europhys. Lett. **13**, 523 (1990).
[22]J. C. Dyre, Phys. Rev. B **48**, 12 511 (1993).
[23]A. Hunt, J. Phys. C **3**, 7831 (1991); **4**, 5371 (1992); J. Non-Cryst. Solids **160**, 183 (1993).
[24]R. Kubo, M. Toda, in N. Hashitsume, *Statistical Physics II* (Springer-Verlag, Berlin, 1985).
[25]A. Abragam, *The Principles of Nuclear Magnetism* (Clarendon, Oxford, 1962).
[26]D. Wolf, *Spin-Temperature and Nuclear-Spin Relaxation in Matter* (Clarendon, Oxford, 1979).
[27]D. Knödler and W. Deiterich, Physica A **191**, 426 (1992).
[28]A. Bunde and S. Havlin, in *Fractals and Disordered Systems*, edited by A. Bunde and S. Havlin (Springer, Heidelberg, 1991).
[29]M. D. Ingram, J. Non-Cryst. Solids **131-133**, 955 (1991).
[30]J. Hoshen and R. Kopelman, Phys. Rev. B **14**, 3438 (1976).
[31]M. P. Allen and D. J. Tildesley, *Computer Simulation of Liquids* (Clarendon, Oxford, 1987).
[32]K. L. Ngai and G. N. Greaves, in *Diffusion in Amorphous Materials*, edited by H. Jain and D. Gupta (The Minerals, Metals, and Materials Society, Warrendale, 1994).
[33]G. H. Weiss, in *Fractals in Science*, edited by A. Bunde and S. Havlin (Springer, Heidelberg, 1994).
[34]H. Scher and M. Lax, Phys. Rev. B **7**, 4491 (1973).
[35]J. W. Haus and K. W. Kehr, Phys. Rep. **150**, 263 (1987).
[36]A. Bunde, S. Havlin, and H. E. Roman, Phys. Rev. A **42**, 6274 (1990).
[37]M. Tatsumisago, C. A. Angell, and S. W. Martin, J. Chem. Phys. **97**, 6968 (1992).
[38]P. Heitjans (private communication).
[39]A. Bunde, P. Maass, and M. Meyer, Physica A **191**, 433 (1992).
[40]M. D. Ingram, in *Material Science and Technology* (VCH Verlagsgesellschaft, Weinheim, 1991), Vol. 9.
[41]P. Maass, A. Bunde, and M. D. Ingram, Phys. Rev. Lett. **68**, 3064 (1992).
[42]A. Bunde, M. D. Ingram, and P. Maass, J. Non-Cryst. Solids **172-174**, 1222 (1994).
[43]V. Jaenisch, M. Meyer, P. Maass, and A. Bunde (unpublished).
[44]W. Küchler, P. Heitjans, A. Payer, and R. Schöllhorn (unpublished).